ELSEVIER

Ceramics International 30 (2004) 883–892

CERAMICS INTERNATIONAL

www.elsevier.com/locate/ceramint

Nanosized alumina from boehmite additions in alumina porcelain 1. Effect on reactivity and mullitisation

F. Belnou, D. Goeuriot*, P. Goeuriot, F. Valdivieso

Ecole Nationale Supérieure des Mines de Saint-Etienne (Centre SMS, CNRS-UMR 5146), 42023 Saint-Etienne Cedex 2, France

Received 11 September 2002; received in revised form 17 October 2003; accepted 17 October 2003

Available online 9 April 2004

Abstract

The influence of nanosized alumina additions and of grain size of alumina filler on the reaction-sintering of alumina porcelain is investigated. Phase and porosity evolution has been studied from room temperature up to 1400 °C. When vitrification occurs the presence of alumina nanoparticles leads to a new type of mullitisation which has two major consequences: a volume expansion resulting in a shrinkage inhibition and a decrease of the amount of liquid which causes densification problems at usual firing temperatures. This phenomenon is enhanced if the alumina filler is coarse but it is limited when fine and round alumina is used because in that last case vitrification kinetics is slowed down.

Keywords: A. Sintering; B. Nanocomposites; D. Mullite; D. Porcelain

1. Introduction

Mullitisation has been studied for decades in a number of systems. It is a complex reaction, not always fully understood yet, whose features (reaction temperature, composition and structure of synthesized mullite, formation mechanisms, etc.) are dependent on many parameters: process and starting materials are never the same towards mullitisation [1].

In alumina porcelains three kinds of mullitisation are generally reported [2–5]. Primary mullitisation occurs first when heating porcelain bodies around 1000 °C [2,4] as the final step of a series of reaction taking place inside kaolin particles [6–9]. Secondary mullite is formed when molten feldspar dissolves alumina rich metakaolinitic relicts [3,5]. The feldspathic liquid can also partially dissolve alumina filler grains and thus form tertiary mullite [2,3,5]: this mechanism is close to that of secondary mullitisation and has been observed in other systems such as kaolinite–alumina mixtures [10–12].

Tertiary mullitisation is the only example of free alumina reactivity towards mullitisation in porcelains: alumina grains that react here are used as filler and are thus not fine (around 1–10 μm). The reactivity of nanosized alumina in porcelainic systems has not been studied yet.

The present work focusses on the influence of additions of alumina filler (0.5–6 μm) and nanosized alumina (boehmite gel) on the reactivity of porcelain: these additions are supposed to strengthen porcelain parts in both green and fired states. The first part of this study is a systematic anisothermal investigation of reactivity within this new porcelainic system. The second part is devoted to the resolution of sintering problems induced by this new formulation and the elaboration of alumina porcelains with better green resistance and sintered thermomechanical properties.

2. Experimental procedures

The materials used in this study are industrial porcelain pastes (kaolin, potash and soda feldspars, chalk) with alumina additions (no quartz is added in the paste): these additions are under the form of granular alumina (alumina filler) for general strengthening and/or boehmite gel for better green mechanical properties [13]. Mixing of all starting products is made via classical wet processing methods [13]: the alumina powder is first dispersed in water with a dispersing agent (ammonium polyacrylate); then the porcelain paste is added; in the case of alumina gel addition, the sol is prepared separately, and added to the precedent slurry; both

* Corresponding author. Tel.: +33-4-7742-0192; fax: +33-4-7742-0249.
E-mail address: dgoeurio@emse.fr (D. Goeuriot).

0272-8842/$30.00
doi:10.1016/j.ceramint.2003.10.009

Table 1
Oxide composition of tested samples (in wt.%)

	Kaolinite phases (wt.%)	Feldspathic phases (wt.%)	Lime (wt.%)	Alumina (including gel) (wt.%)	Wt.% in the paste
SiO_2	56.4	68.1	<0.1	–	41
Al_2O_3	40.4	18	<0.1	>99.8	52.3
Alkalis (K_2O, Na_2O)	2.3 1.7 0.6	12.3 Major phase Minor phase	–	–	3.9 Major phase Minor phase
Others	Oxides 0.9 (Fe_2O_3, TiO_2, Li_2O, MgO, CaO) Water	Oxides 1.6 (Fe_2O_3, TiO_2, Li_2O, MgO, CaO)	$CaCO_3$: 99.1; MgO: 0.5; Fe_2O_3: <0.2	Oxides (<0.2) (Na_2O, Fe_2O_3, SiO_2)	Oxides: 0.8 $CaCO_3$: 2
Size	70% < 2 μm	50% < 17 μm	50% < 30 μm	Coarse: 50% < 4–6 μm fine: 50% < 0.5 μm gel: SS: 180 m^2/g	–
Wt.% in the paste	45	23	2	30	100

gelling and mixing are performed simultaneously. Samples are extruded. Two types of alumina filler are used: a fine one (d_{50} = 0.48 μm) and a coarse one (d_{50} = 4–6 μm). Three types of mixtures of the same chemical composition (see Table 1) are investigated, PC, PCG and PFG: details on the nature of mixed starting products are given in Table 2; the compositions are given before firing for the porcelain paste minerals (for example, $CaCO_3$), but the percentage of gel corresponds to the added alumina (the dehydratation is taken into account for the calculations).

Dilatometry experiments are performed with Setaram TMA92 apparatus under reconstituted air flow at 5 °C min^{-1} up to 1400 °C. Infra-red spectra are obtained on Bruker Equinox 55 spectrometer. X-ray diffraction measurements are made with Siemens D5000 diffractometer on specimens heated in a Naberthem furnace (when a soaking is performed, dwell time is indicated in Table 3) and quenched in water: quantifications from XRD spectra are based on the peaks surface areas: (1 1 0), (0 0 6) and (1 1 3) peaks are used for the quantification of α-alumina, (2 2 0) and (1 2 1) peaks for mullite, (1 0 0) peak for quartz, a series of small peaks in the range $(2|\bar{2}|0)$ to $(2|\bar{1}|\bar{4})$ for anorthite; the intensity of each peak I_a $(h\,k\,l)$ mentioned before depends on the quantity V_a of the a phase, on a structural factor i $(h\,k\,l)$, and others factors that are constant for all analyses (beam absorption by the solid, beam wave length and area). So the volume ratio V_a of each phase under the total volume of crystallized phases can be determined:

$$V_a = \frac{I_a^{hkl}/i_a^{hkl}}{\sum_y^x (I_y^x/i_y^x)} \quad (1)$$

Table 2
Details and green densities of the three types of mixtures (in wt.%)

	PC	PCG	PFG
Porcelain[a]	70	70	70
Coarse Al_2O_3[b]	30	20	–
Fine Al_2O_3[b]	–	–	20
Boehmite gel	–	10	10
Green density	1.98 ± 0.04	1.83 ± 0.02	1.77 ± 0.04

[a] Kaolin 64.3 wt.%, feldspar 32.9 wt.% (microcline + albite) and chalk 2.8 wt.%.
[b] Coarse d_{50} = 4–6 μm, fine d_{50} = 0.48 μm.

Table 3
Phases contents in the three studied materials at various temperatures (in wt.%): error: ±2% for major phases and ±1% for minor phases

Thermal cycle	PC	PCG	PFG
1200 °C 20 min	Alumina 35 Mullite 19 Quartz 4 Anorthite 5 Glass 37	Alumina 26 Mullite 30 Quartz 6 Anorthite 4 Glass 34	Alumina 29 Mullite 19 Quartz 4 Anorthite 2 Glass 46
1200 °C 40 min	–	Alumina 27 Mullite 33 Quartz 7 Anorthite 3 Glass 30	Alumina 29 Mullite 19 Quartz 3 Anorthite 2 Glass 47
1250 °C 0 min	Alumina 35 Mullite 16 Quartz 1 Anorthite 2 Glass 46	Alumina 29 Mullite 29 Quartz 4 Anorthite 3 Glass 35	Alumina 30 Mullite 19 Quartz 2 Anorthite 3 Glass 46
1300 °C 0 min	Alumina 35 Mullite 16 Quartz 5 Anorthite 0 Glass 44	Alumina 28 Mullite 31 Quartz 4 Anorthite 3 Glass 34	Alumina 32 Mullite 20 Quartz 2 Anorthite 2 Glass 44

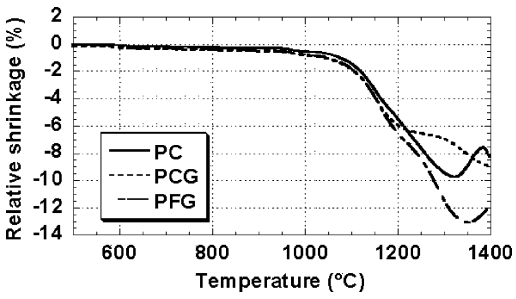

Fig. 1. Dilatometric behaviour of the materials with temperature.

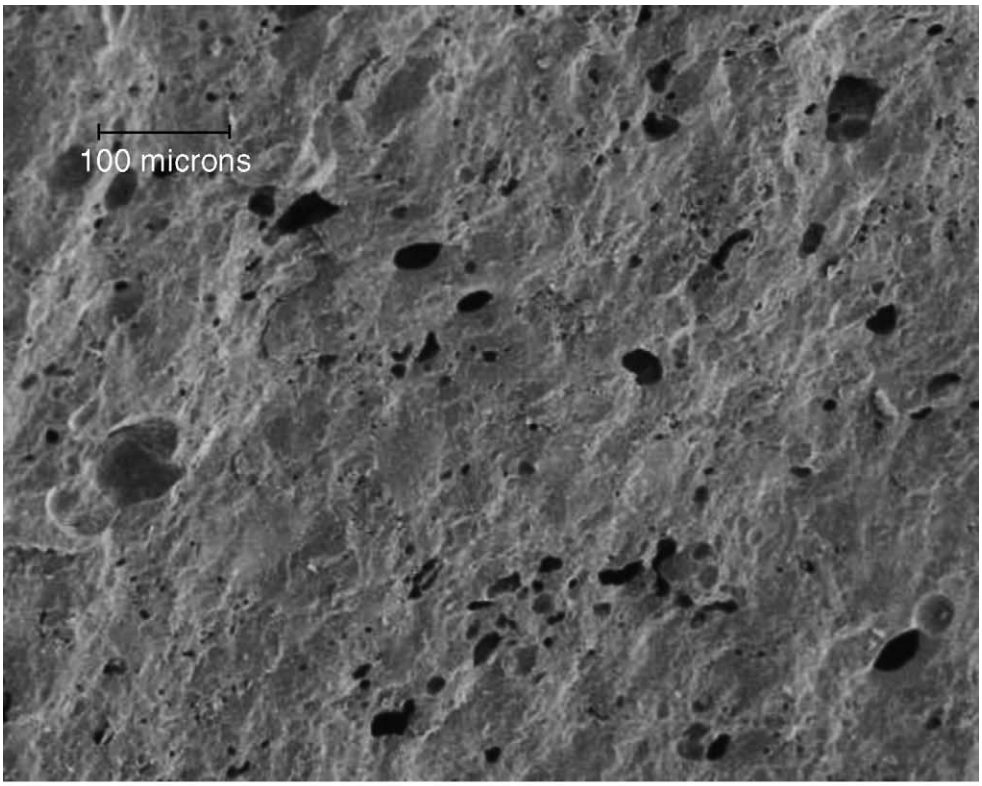

(a)

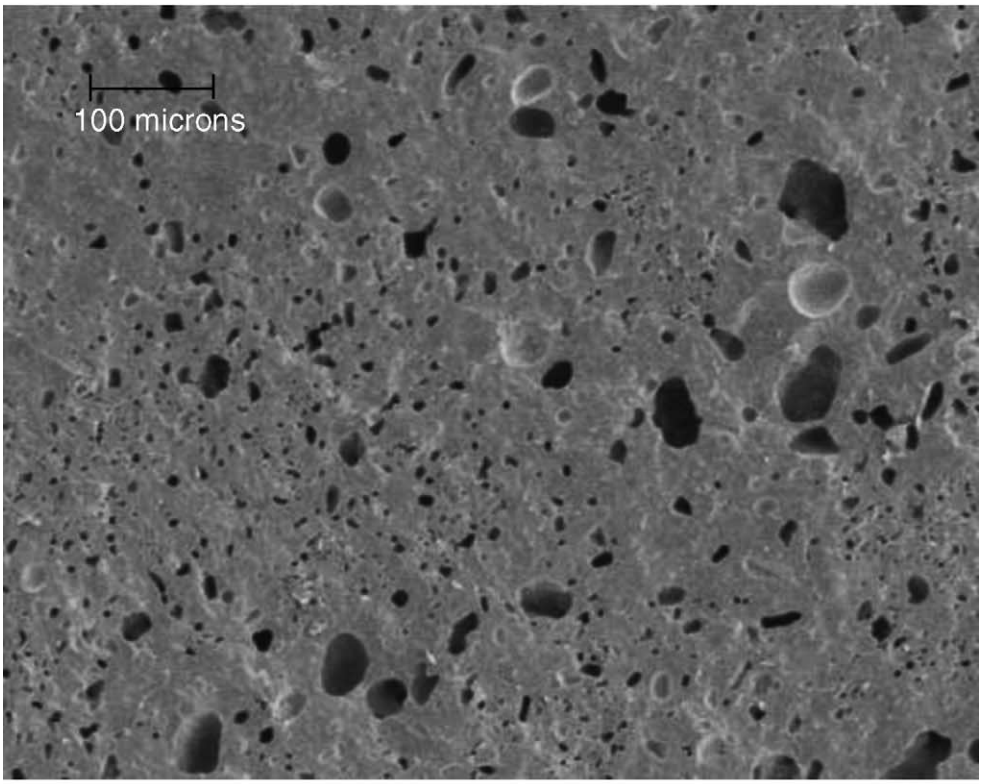

(b)

Fig. 2. Comparison of the densification achieved in (a) PC at 1300 °C and (b) PCG at 1400 °C.

where I ($k\,k\,l$) is given by the software CaRine Cristallography 3.1; by using several peaks a mean V_a can be calculated. The complementary amount of liquid/glass is estimated by HF dissolution method [14] (a small quantity of nanocrystals are dissolved by HF and are thus part of the glass amounts given in this paper). From the glass content and the different V_a, an approximate composition (error ±2% for major phases and 1% for minor phases in Table 3) for each sample is then determined. Microstructural investigations are made on Jeol JSM840 SEM and Philips CM200 TEM.

3. Results and discussion

3.1. Shrinkage inhibition

The dilatometric curves presented on Fig. 1 reveal that shrinkage occurs in each material but is inhibited in the range 1150–1250 °C: this phenomenon is enhanced when gel (nanosized alumina) is contained in the tested paste and as the grain size of alumina filler increases. It can be noticed that the green densities of the three samples are quite different (Table 1), that could influence shrinkage; despite these differences, shrinkage inhibition is visible for the three materials. The micrographs of Fig. 2 show that the combination of both gel and coarse alumina also results in a lack of densification at high temperatures. To know if these two results are directly linked porosity measurements are done on samples heated at different temperatures and quenched in water.

3.2. Porosity removal

It is well known than in these kind of materials pore elimination occurs via migration into glass because of vitrification. As mentioned above, Table 1 indicates that the three materials initially have different green densities: this appears on Fig. 3 which shows a difference in the amount of porosity between the three materials. Fig. 3 also indicates that porosity elimination proceeds at the same rate in the three materials up to 1250 °C: above 1250 °C, it accelerates in PFG. The initial porosity difference is maintained throughout the thermal cycle despite significant disparities in shrinkage behaviour: this means that the shrinkage inhibition observed on the dilatometric curves is not linked to a densification inhibition.

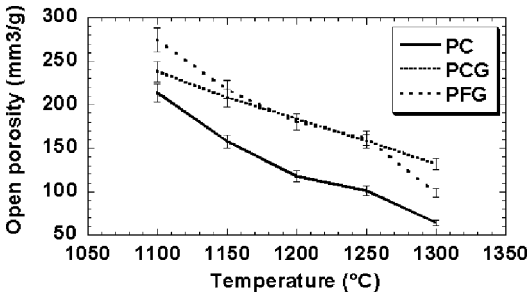

Fig. 3. Evolution of open porosity with temperature.

3.3. Phase evolution under 1150 °C

At around 990 °C, primary mullitisation occurs as indicated on shrinkage curves by a small peak. However, mullite is not detected by XRD until 1100–1150 °C as shown on Fig. 4. This is because metakaolin decomposition first gives birth to a premullitic system, composed of nanocrystalline particles of mullite and/or γ-alumina or aluminium–silicon spinel [6–9] that can only be detected by XRD when substantial growth has occurred [4,9].

Fig. 4 also indicates that alumina filler and quartz remain inert and that feldspar has partially melted at 1150 °C (albite peaks have disappeared, only microcline and traces of anorthite are detected).

Up to 1150 °C phase evolution is the same as can be expected in a classical porcelain system and does not seem to be influenced by alumina additions (filler and gel).

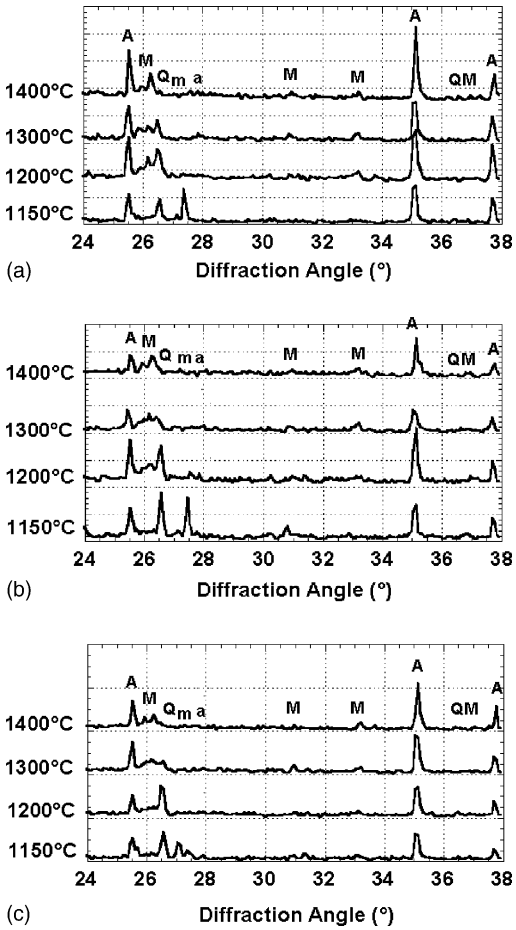

Fig. 4. Phase evolution with temperature for (a) PC, (b) PCG and (c) PFG (A: α-alumina, M: mullite, Q: quartz, m: microcline, a: anorthite).

3.4. Phase evolution above 1150 °C

3.4.1. Vitrification

In Fig. 4 microcline disappears between 1150 and 1200 °C because it decomposes into leucite and glass [15]. In porcelain leucite remains dissolved into glass, so microcline disappearance is the last step of global vitrification. Amorphous phases are very inhomogeneous and consist of zones of various viscosities ranging from highly viscous and almost pure silica glass to low viscosity feldspathic liquid.

3.4.2. Mullitisation

Fig. 4 and Table 3 indicate that mullitisation proceeds up to 1200 °C and stops, except for PC where a small decrease is recorded: a part of primary mullite can thus be dissolved by liquid as it has been observed previously [4]. PCG is the richest in mullite: systematic TEM observations of thin foils from materials heated at 1200 and 1250 °C confirm this result. Fig. 5 shows some nanometric mullite crystals in a glassy matrix, with acicular shape and square section. In some areas of the thin sections needles are smaller and less numerous than on this micrograph, indicating differential mullitisation throughout the samples.

The main difference between the three materials is the amount of produced mullite. The first mullite formed is primary mullite in metakaolin: as the quantity of kaolin introduced is the same in all three materials, this should not lead to different primary mullite contents. No direct evidence of secondary mullite formation between 1150 and 1250 °C has been found but if this happens it should also be in the same proportions in every materials for the same reasons.

In fact these materials differ by the size of alumina filler and the presence of gel. Alpha alumina peaks on Fig. 4 and associated quantities given in Table 3 do not change

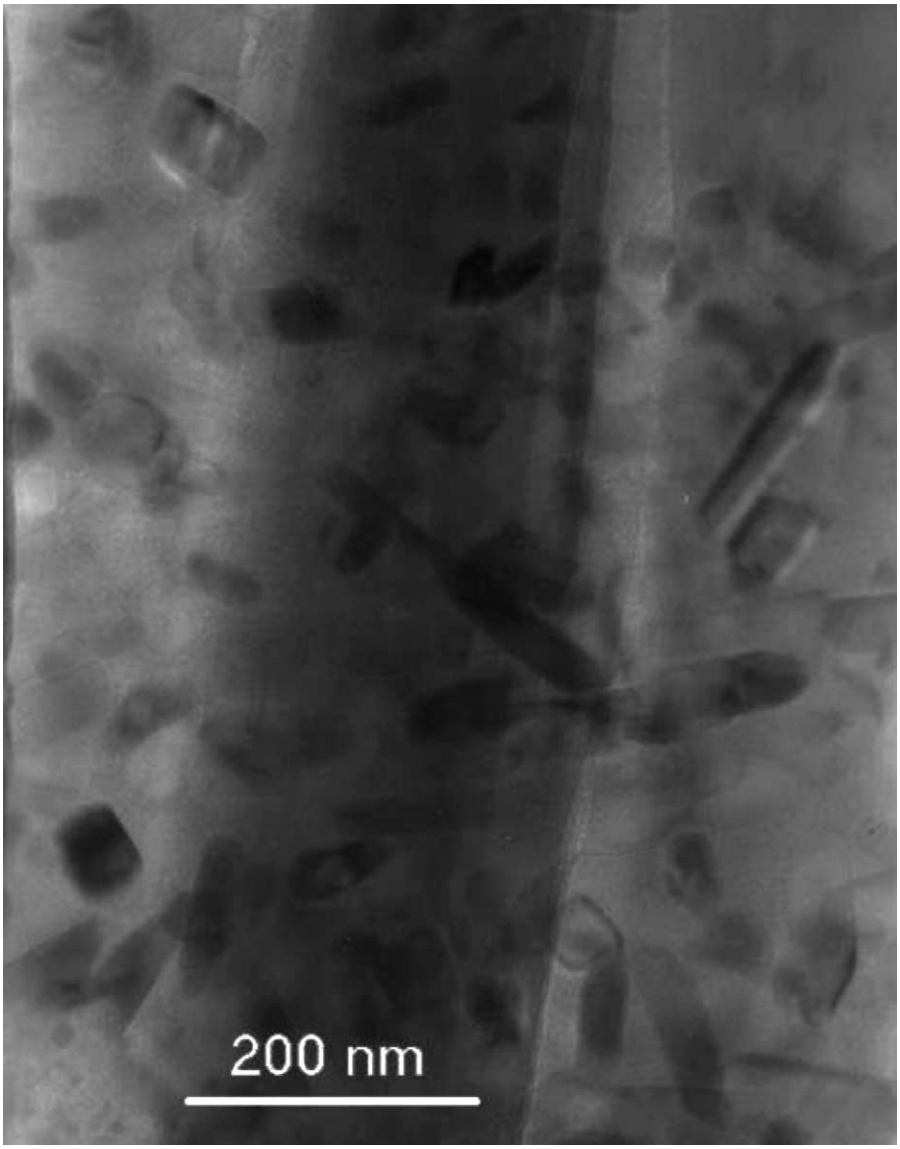

Fig. 5. Mullite crystals embedded in glass: square sections of the needles are visible (PC heated up to 1200 °C and quenched).

significantly with temperature which suggests that alumina filler remains inert: it thus does not participate to mullite formation. The two gel containing materials are richer in mullite: as liquid/glass is too alumina poor to mullitise, it is likely that it can dissolve ex-gel alumina so that mullite precipitates. This mechanism is close to that leading to tertiary mullite by dissolution of alumina in the liquid. For that it will be called pseudotertiary mullitisation. This phenomenon occurs at high temperature in alumina rich porcelains [3–5]; in the present work, it can be supposed to happen at lower temperature because of the high reactivity of alumina gel.

But such a mechanism does not explain the great difference in mullite content in PCG and PFG (same gel content). Fig. 6 shows that alumina dispersion is heterogeneous. This is due to the initial mixing: the smaller alumina and kaolin grains have been brought together around the larger feldspar particles and this configuration remains up to high temperature. This phenomenon is especially developed in PFG, as shown on Fig. 7, where alumina grains are aggregated because of their small size. Because of this particular dispersion, after feldspar melting liquid has to cross alumina rings to spread within the samples: these rings act as a barrier which is especially strong in PFG where grains are aggregated. This results in slower kinetics for pseudotertiary mullitisation in PFG.

3.4.3. Alumina

As shown in previous paragraph, alumina filler is inert: 1400 °C is not a sufficient temperature to induce alumina dissolution by the feldspathic liquid, which is consistent with authors observations in related systems [2,3,5,10–12]. High measured contents given in Table 3 are due to the dehydroxylation of kaolinite and decomposition of limestone.

Note that the alumina content is smaller for PCG and PFG due to partial substitution of alumina filler by gel: the particles of boehmite have transformed into nanocrystalline γ-alumina, not detected by XRD. Above 1150 °C, this γ-alumina should become α-alumina and its content in PCG and PFG should reach the value obtained in PC. However, this is not the case as this γ-alumina is consumed during pseudotertiary mullitisation. In PFG where this reaction is inhibited, there is significantly more alumina than in PCG because unreacted gel transforms into α-alumina in the temperature range 1200–1250 °C: these high temperatures for γ–α transformation are due to the presence of amorphous silica which delays alumina transitions [16,17]. Pseudotertiary mullitisation and gel transformation are competitive processes.

3.4.4. Metakaolin

TEM observations show large areas of nanocrystals diffracting as γ-alumina (see Fig. 8). These areas can be seen in PC which does not contain gel, providing evidence that metakaolinitic relicts can remain at temperatures as high as 1200–1250 °C. Silicon is always detected by EDS in these areas but the method's resolution has not allowed us to isolate a single crystal: so only further investigations could help to determine the exact nature of each observed

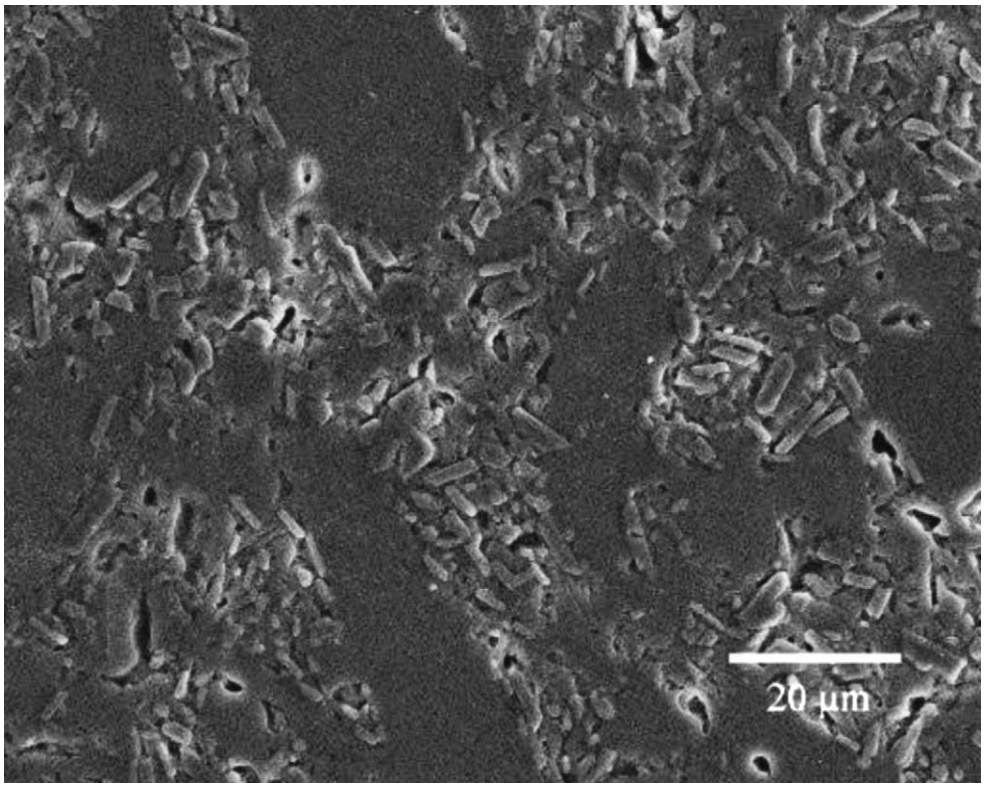

Fig. 6. Alumina dispersion in matrix: the shape of the original kaolin grains appears (PCG).

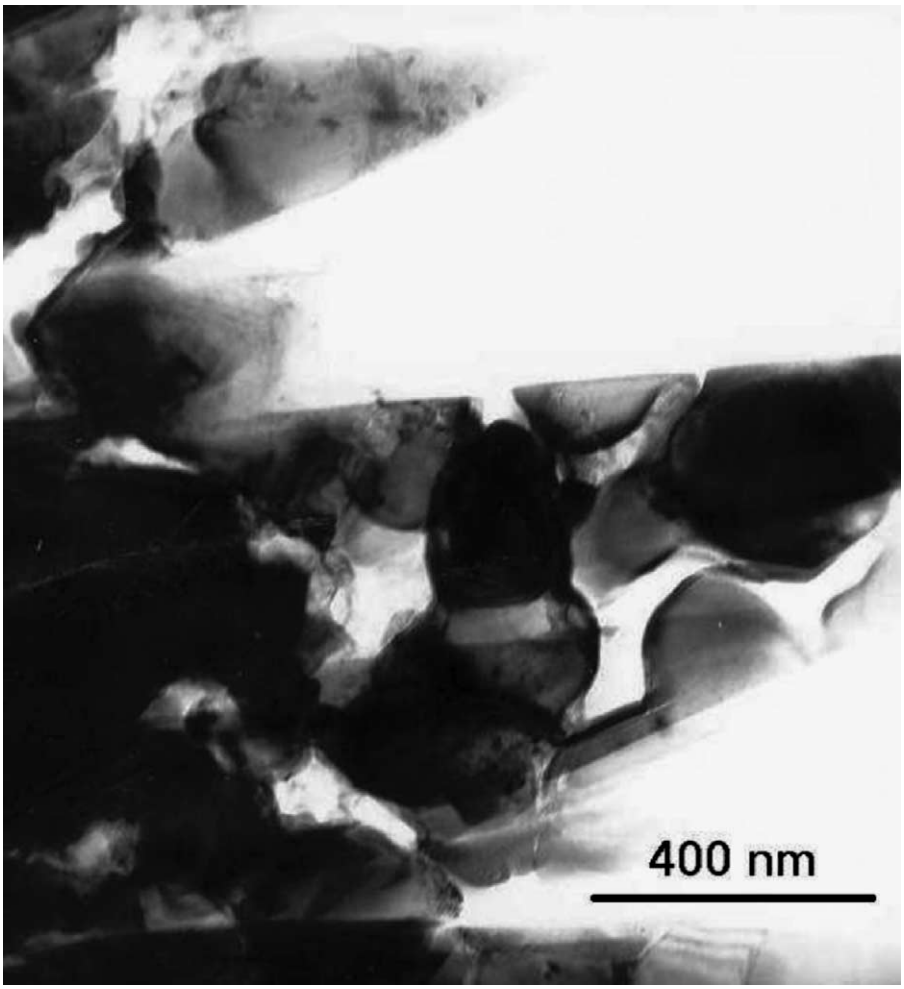

Fig. 7. Alumina grains aggregated in PFG (heated up to 1200 °C and quenched).

areas, γ-alumina or aluminium-silicon spinel. Fig. 9 shows an example of one of these zones in PC which is part of a metakaolinitic relict.

3.4.5. Anorthite

A significant amount of anorthite is found that clearly diminishes with temperature and has disappeared in every materials at 1400 °C, as shown in Fig. 4 and Table 3. Comparison of anorthite quantities in the three materials is difficult and can be within the range of experimental error (±1%).

Chalk incorporated into liquid phase is the only source of CaO in our system. According to the $CaO–Al_2O_3–SiO_2$ phase diagram [15], anorthite crystallisation from liquid can occur above 1165 °C for certain compositions (when liquid phase becomes richer in alumina). The anorthite-potash feldspar phase diagram [15] indicates that feldspar rich anorthite–feldspar mixtures lead to leucite and liquid at temperatures depending on the composition. Anorthite is thus a transitory phase that crystallises from a CaO containing liquid and is then dissolved by feldspathic liquid.

The $CaO–Al_2O_3–SiO_2$ phase diagram indicates that anorthite formation is preferential to mullitisation. As the mechanism of these two reactions is similar (alumina dissolution), anorthite formation can thus limit both types of secondary mullitisation: this phenomenon is clearly put in evidence in the second part of this study [13].

3.4.6. Quartz

Quartz dissolution in the liquid clearly appears on Fig. 4 and Table 3: it is though limited in PCG up to high temperature.

3.4.7. Liquid/glass

Liquid/glassy phase is generalised above 1150 °C and includes amorphous silica and feldspar. For that reason, it is heterogeneous: some areas approximate the composition of pure silica, others contain varied quantities of alkalis, and crystal free and mullite containing areas have different compositions.

The lack of liquid/glassy phase in PCG (see Table 3) is induced by extra mullitisation and explains that quartz dissolution and final densification are limited in this material. It is also possible that differential crystallisation induces a local modification of the viscosity of liquid phase which can

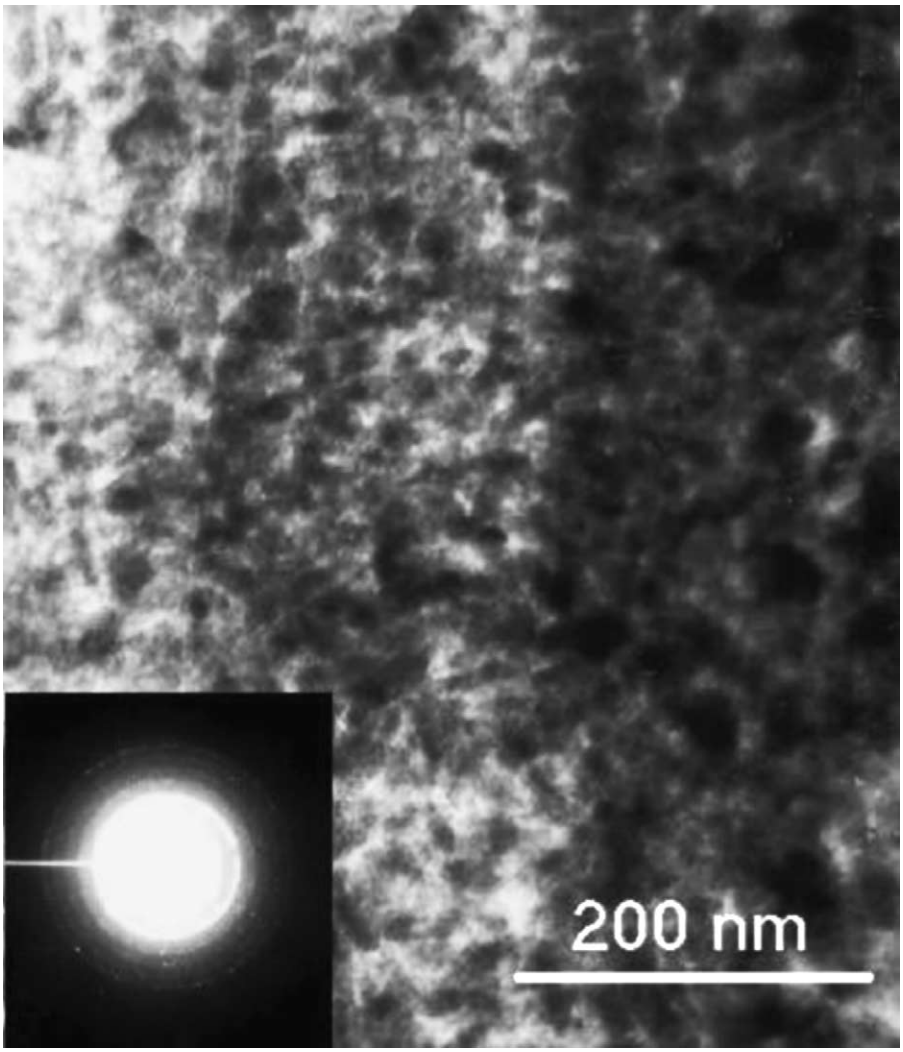

Fig. 8. An agglomerate of γ-alumina nanocrystals (PCG heated up to 1250 °C and quenched).

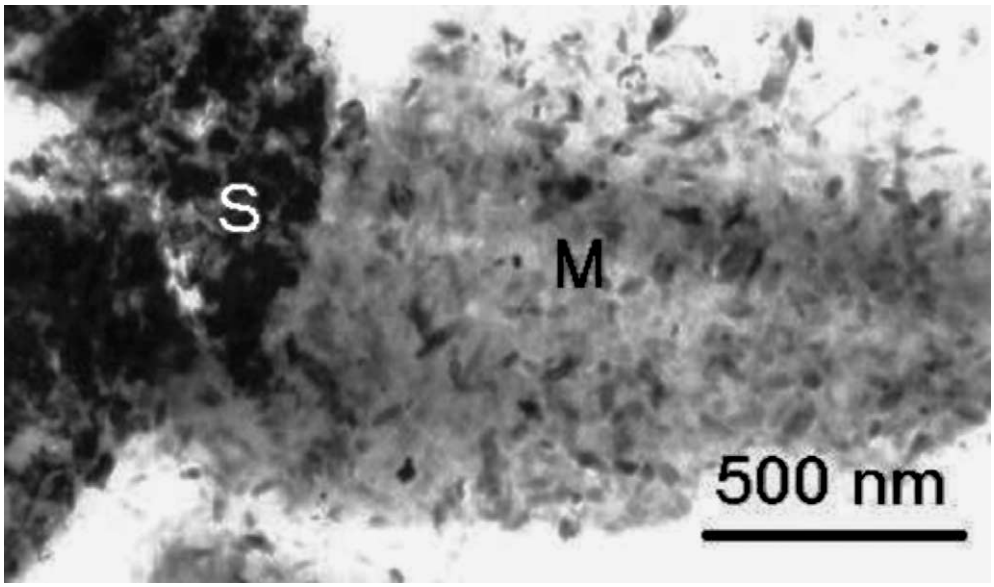

Fig. 9. Adjacent mullitic (M) and spinel-type (S) zones suggesting a metakaolinitic relict (PC heated up to 1200 °C and quenched).

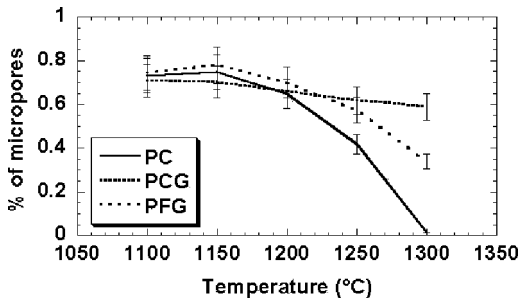

Fig. 10. Evolution of the ratio of micropores in total porosity with temperature.

affect densification: however, this possibility has not been confirmed by our investigations.

3.5. Pore coalescence

Closer examination of porosity data shows that differential microporosity ($\varnothing < 1\,\mu m$) evolution hides behind a similar global porosity elimination behaviour. At high temperatures, the relative quantity of micropores decrease in PFG and PC (especially in PC where micropores disappear at 1300 °C), as showed on Fig. 10. This diminution can be correlated with the vitrification of the system around 1150 °C and is the result of both global porosity removal and coalescence of some of the remaining pores. Coalescence is delayed in PFG as liquid spreading kinetics is limited by the alumina barrier effect. It does not take place in PCG because it is the poorest in liquid phase.

3.6. Mullitisation and shrinkage inhibition

The temperature range associated with shrinkage inhibition corresponds to intense mullitisation. Other authors have noticed the detrimental effect of mullitisation on shrinkage in other materials [18,19]: in alumina–zircon mixtures this has been attributed to a volume expansion associated to the reaction [20,21]. This study has shown that nothing can be correlated with the sharpness of shrinkage inhibition except the amount of mullite, from which a part comes from the dissolution of nanosized alumina by the liquid phase. Considering this and the converging results in literature, this phenomenon of shrinkage inhibition is probably linked to a volume increase associated to pseudotertiary mullitisation. The volume expansion cannot be calculated because it seems impossible to determine the glass volume mass, but it seems plausible considering the high density of alumina ($4\,g/cm^3$), converted in mullite ($3.2\,g/cm^3$).

4. Conclusions

In low temperature range, the phase evolution of alumina porcelains containing nanosized alumina is similar to that of classical porcelain systems. Vitrification is completed above 1150 °C with the end of feldspar melting and the beginning of quartz dissolution.

In the range 1150–1250 °C, additional mullitisation occurs when nanosized alumina is present in the system (gel containing materials) through a mechanism that is very similar to that of tertiary mullitisation: nanosized alumina is dissolved by liquid phase and mullite precipitates. For that reason this special kind of mullitisation is called pseudotertiary mullitisation. Unreacted gel finally transforms into α-alumina: as this reaction lies in the same temperature range it is competitive with pseudotertiary mullitisation.

The grain size and shape of alumina filler have an influence on liquid phase spreading inside the samples: when grains are fine and round they are aggregated and act as barriers which slow liquid spreading down. This results in pseudotertiary mullitisation inhibition and gel transformation enhancement when fine alumina filler is combined with boehmite gel.

Shrinkage inhibition between 1150 and 1250 °C does not correspond to densification inhibition but is probably caused by a volume expansion which accompanies pseudotertiary mullitisation. Thus limited final densification in the material containing boehmite gel and coarse alumina filler is not a direct consequence of greater shrinkage inhibition: it occurs because enhanced secondary mullitisation II in this material finally leads to a lack of liquid phase which hinders it to fill the initial porosity gap that separates it from the two other materials.

Acknowledgements

The authors would like to thank Groupe Cerama and Région Rhônes-Alpes for financial support of this study.

References

[1] I.A. Aksay, D.M. Dabbs, M. Sarikaya, Mullite for structural, electronic and optical applications, J. Am. Ceram. Soc. 74 (10) (1991) 2343–2358.
[2] W.M. Carty, U. Senapati, Porcelain—raw materials, processing, phase evolution and mechanical behavior, J. Am. Ceram. Soc. 81 (1) (1998) 3–20.
[3] Y. Iqbal, W.E. Lee, Fired porcelain microstructures revisited, J. Am. Ceram. Soc. 82 (12) (1999) 3584–3590.
[4] Y. Iqbal, W.E. Lee, Microstructural evolution of triaxial porcelain, J. Am. Ceram. Soc. 83 (12) (2000) 3121–3127.
[5] W.E. Lee, Y. Iqbal, Influence of mixing on mullite formation in porcelain, J. Eur. Ceram. Soc. 21 (2001) 2583–2586.
[6] G.W. Brindley, M. Nakahira, The kaolinite–mullite reaction series, J. Am. Ceram. Soc. 42 (7) (1959) 311–324.
[7] I.W.M. Brown, K.J.D. MacKenzie, M.E. Bowden, R.H. Meinhold, Outstanding problems in the kaolinite–mullite reaction sequence investigated by ^{29}Si and ^{27}Al solid-state nuclear magnetic resonance: II. High temperature transformations of metakaolinite, J. Am. Ceram. Soc. 68 (6) (1985) 298–301.
[8] K. Srikrishna, G. Thomas, R. Martinez, M.P. Corral, S. De Aza, J.S. Moya, Kaolinite–mullite reaction series: a TEM study, J. Mater. Sci. 25 (1990) 607–612.

[9] S. Lee, Y.J. Kim, H.S. Moon, Phase transformation sequence from kaolinite to mullite investigated by an energy-filtering transmission electron microscope, J. Am. Ceram. Soc. 82 (10) (1999) 2841–2848.
[10] K.C. Liu, G. Thomas, A. Caballero, J.S. Moya, S. De Aza, Mullite formation in kaolinite–α-alumina, Acta Metall. Mater. 42 (2) (1994) 489–495.
[11] C.Y. Chen, G.S. Lan, W.H. Tuan, Preparation of mullite by the reaction-sintering of kaolinite and alumina, J. Eur. Ceram. Soc. 20 (2000) 2519–2525.
[12] M.A. Sainz, F.J. Serrano, J.M. Amigo, J. Bastida, A. Caballero, XRD microstructural analysis of mullites obtained from kaolinite–alumina mixtures, J. Eur. Ceram. Soc. 20 (2000) 403–412.
[13] F. Belnou, Mullitisation and shrinkage inhibition in multioxyde systems, PhD thesis, Saint-Etienne, 2002.
[14] W.C. Zhou, L.T. Zhang, H.Z. Fu, Modification of the hydrofluoric acid leaching technique: I. Corundum–mullite–glassy phase materials, J. Am. Ceram. Soc. 71 (5) (1988) 395–398.
[15] E.M. Levin, C.R. Robbins, H.F. McMurdie, Phase diagrams for ceramists, The American Ceramic Society Inc., 1st ed., figs. 412, 788, 501, 631 and 799 (by order of appearance in the main text), 1964.
[16] W.C. Wei, J.W. Halloran, Phase transformation of diphasic aluminosilicate gels, J. Am. Ceram. Soc. 71 (3) (1988) 166–172.
[17] D.X. Li, W.J. Thomson, Kinetic mechanisms for mullite formation from sol–gel precursors, J. Mater. Res. 5 (9) (1990) 1963–1969.
[18] C.F. Chan, Y.C. Ko, Effect of rare-earth oxide concentrate on reaction, densification and slag resistance of Al_2O_3–SiO_2 ceramic refractories, Ceram. Int. 20 (1994) 31–37.
[19] B. Saruhan, U. Voss, H. Schneider, Solid-solution range of mullite up to 1800 °C and microstructural development of ceramics, J. Mater. Sci. 29 (1994) 3261–3268.
[20] A. Leriche, P. Descamps, F. Cambier, Frittage réaction et applications aux composites à dispersoïdes, in: Forceram (Céramiques Composites à Particules, Cas du Frittage-Réaction), Editions Septima, 1992, pp. 9–38 (in French).
[21] V. Yaroshenko, D.S. Wilkinson, Sintering and microstructure modification of mullite/zirconia composites derived from silica-coated alumina powders, J. Am. Ceram. Soc. 84 (4) (2001) 850–858.